Title
THE NUCLEAR ORIENTATION OF 253Es IN NEODYMIUM ETHYLSUL-FATE

Authors
Soinski, A.J.
Frankel, R.B.
Navarro, Q.O.
et al.

Publication Date
1970-04-01

Submitted to Physical Review

UCRL-19576
Preprint

c.2

THE NUCLEAR ORIENTATION OF ^{253}Es IN NEODYMIUM ETHYLSULFATE

A. J. Soinski, R. B. Frankel, Q. O. Navarro,
and D. A. Shirley

April 1970

AEC Contract No. W-7405-eng-48

LAWRENCE RADIATION LABORATORY
UNIVERSITY of CALIFORNIA BERKELEY

DISCLAIMER

THE NUCLEAR ORIENTATION OF ^{253}Es IN NEODYMIUM ETHYLSULFATE*

A. J. Soinski, R. B. Frankel†, Q. O. Navarro††, and D. A. Shirley

Lawrence Radiation Laboratory
University of California
Berkeley, California 94720

April 1970

ABSTRACT

Einsteinium-253 nuclei were oriented at low temperatures in a neodymium ethylsulfate lattice. From the temperature-dependent alpha particle angular distribution a nuclear magnetic moment $\mu = 2.7 \pm 1.3$ nm was deduced. From the values for the angular distribution function at the lowest temperatures it was possible to test the predictions of the Mang shell model theory for the relative phases and amplitudes of the alpha partial waves. As predicted, the waves of angular momentum L = 0 and 2 are in phase and the L = 0 and 4 waves are out of phase. The predicted wave amplitudes are in error, especially that of the L = 4 wave. The predicted relative intensities (which are proportional to the amplitudes squared) for the S, D and G waves are 1.000/0.179/0.0058 whereas the experimental relative intensities are 1.000/0.216/0.0084.

INTRODUCTION

An alpha particle emitted by the ground state of an even-even nucleus has a unique angular momentum, L. The parent nucleus has $I_i = 0$, and angular momentum conservation requires that the daughter energy level populated by the alpha particle should have $I_f = L$. For odd-odd or odd mass nuclei, $I_i \neq 0$ and various values of L are generally permitted. On the basis of angular momentum conservation, Spiers[1] predicted that anisotropic alpha particle emission would take place from oriented nuclei. Subsequent nuclear orientation experiments confirmed this prediction and also yielded information about the relative amplitudes and phases of the observed alpha partial waves.

Hill and Wheeler[2] made the first quantative estimate of enhanced alpha particle emission from the poles of prolately deformed spheroidal nuclei. Their reasoning can be understood with the aid of Fig. 1. They assumed a uniform probability of alpha particle formation within the nuclear volume. If the barrier set up by the remaining nucleons is simply coulombic beyond a given radius, then this barrier is both thinner and lower at the poles than it is at the equator, and tunneling is greatly enhanced at the poles. For moderate nuclear deformation they predicted a sixteen-fold increase of alpha particle intensity from the poles over that from the equator. However, the angular distribution of nuclear radiations is determined primarily by the requirement that angular momentum be conserved in the nuclear decay. The greatly enhanced polar emission predicted by Hill and Wheeler could occur only from a nucleus with a large component of angular momentum perpendicular to the nuclear symmetry axis.

Roberts, Dabbs and co-workers[3-5] were the first to test the predictions of Hill and Wheeler experimentally. They oriented ^{233}U and ^{235}U in single

crystals of $UO_2Rb(NO_3)_3$ and ^{237}Np in single crystals of $NpO_2Rb(NO_3)_3$. For all three nuclei they observed preferential emission perpendicular to the crystalline c-axis. In the ^{237}Np case they were able to establish that the nuclear spins also tend to orient perpendicular to the c-axis. These two facts taken together imply preferential emission along the nuclear spin vector (i.e., from the poles), thus confirming the predictions of Hill and Wheeler. The data for the uranium isotopes are consistent with this interpretation of the ^{237}Np results, although for uranium the direction of orientation was not established directly. Chasman and Rasmussen[6] have discussed the difficulties in interpreting the ^{233}U data.

Navarro et al.[7] aligned trivalent ^{249}Cf in a single crystal of neodymium ethylsulfate $Nd(C_2H_5SO_4)_3 \cdot 9H_2O$, which we shall abbreviate below as NES; Navarro et al. and also Frankel[8] aligned ^{253}Es in NES. For both isotopes the prediction of Hill and Wheeler was confirmed: preferential alpha particle emission from the nuclear poles was observed. Preferential polar emission in these cases reflects the fact that the S and D alpha waves (corresponding to orbital angular momenta L = 0 and 2) are in phase, while preferential equatorial emission would imply that the S and D waves were out of phase. In this paper we report an extension of the ^{253}Es nuclear orientation studies to determine the relative phase of the S and G (L = 4) waves. In a future paper nuclear orientation studies of ^{241}Am and ^{225}Fm in NES are reported.

THEORY

Nuclear orientation has been treated in a number of review articles,[9-13] and we shall discuss only those aspects of the method that are especially pertinent to alpha particle angular distributions. The angular distribution function is essentially a consequence of the law of conservation of angular momentum applied to nuclear radiations. For alpha particles the angular distribution function can be written as

$$W(\theta) = 1 + \sum_{k>0} \sum_{L,L'} a_L a_{L'} \cos(\phi_L - \phi_{L'}) \, b_k(LL'I_f I_i) \, F_k(LL'I_f I_i) \, B_k(I_i,T) \, P_k(\cos\theta) \Big/ \sum_L |a_L|^2 \quad , \tag{1}$$

where a_L is the relative amplitude and ϕ_L the relative phase of the L-alpha wave. The parameter F_k is familiar from γ-ray angular correlation theory, and $b_k(LL'I_f I_i)$ is a particle parameter which reflects the fact that alpha particles are spin-zero bosons. Only even-k terms are nonzero for parity-conserving processes.

The orientation parameters B_k are statistical tensors which describe the populations of the nuclear magnetic substates. They contain all the solid state physics information, and the entire temperature dependence, in $W(\theta)$. The P_k's are the Legendre polynomials with the angle θ measured between the crystalline c-axis and the direction of alpha particle emission.

Because the product of the particle parameter and an F coefficient is proportional to the product of a $3j$ symbol and a $6j$ symbol

$$b_k(LL'I_fI_i)\, F_k(LL'I_fI_i) = \tag{2}$$

$$(-1)^{I_i+I_f}\sqrt{(2L+1)(2L'+1)(2I_i+1)(2k+1)}\begin{pmatrix} L & L' & k \\ 0 & 0 & 0 \end{pmatrix}\begin{Bmatrix} L & L' & k \\ I_i & I_i & I_f \end{Bmatrix},$$

the angular distribution can be written as

$$W(\theta) = 1 + A_2(LL'I_fI_i)\, B_2(I_i,T)\, P_2(\cos\theta) + A_4(LL'I_fI_i)\, B_4(I_i,T)\, P_4(\cos\theta) \tag{3}$$

which shows that each angular distribution coefficient can be factored into two terms. The summation over k is restricted to $k = 2,4$ for this case because $A_6(LL'I_fI_i)$ is less than $0.02\, A_4(LL'I_fI_i)$ and hence can be neglected. Higher order terms are zero because of the properties of the $6j$ symbol. The A_k term depends specifically on the decaying nucleus, while the B_k term depends on both the (hyperfine) interaction of the nucleus with its environment and the temperature. We will treat these two terms in order, first considering the alpha decaying nucleus and then consider the solid state aspects.

The conservation of angular momentum restricts L to $|I_i - I_f| \leq L \leq I_i + I_f$ where I_i and I_f are the spins of the parent and daughter nucleus respectively. The conservation of parity further restricts L to even (odd) values if the parent and daughter have the same (opposite) parity. The relative amplitudes of the alpha waves can be obtained from the reduced transition probabilities calculated according to the prescription of Bohr, Fröman and Mottelson,[14] which we will abbreviate below as BFM. The

projection K of total angular momentum along the nuclear symmetry axis is nearly a constant of motion for most spheroidal nuclei. For odd-mass nuclei, transitions for which $\Delta K = 0$ are favored: these transitions do not involve the last odd nucleon and do not require the breaking of pairs. Mang et al.[15] have shown that pairing correlations have a decisive influence on alpha decay transition rates.

As a consequence of the Wigner-Eckart theorem the transition matrix elements for a given alpha partial wave populating various rotational states of the daughter will vary, according to the BFM model, as the ratio of Clebsch-Gordan coefficients. The reduced transition probability or decay constant $\lambda = \frac{\ell n 2}{t_{1/2}}$ will then be proportional to the product of (the square of a Clebsch-Gordan coefficient) times (the reciprocal of a hindrance factor averaged from neighboring even-even nuclei) times (a barrier penetration factor). The predicted partial wave intensities for the favored transitions of ^{253}Es are given in Table I. A partial decay scheme, as adapted from Ref. 16, is given in Fig. 2.

The BFM prediction is exact only in the limit of infinite nuclear moment of inertia and vanishing nuclear quadrupole moment. Because the actinides typically have large quadrupole moments, deviations from the BFM predictions are expected. More accurate values for the decay constants and hence for the partial wave amplitudes can be obtained by solving either a three-dimensional non-separable Schrödinger equation or a set of coupled differential equations for the radial wave functions. Mang's shell model theory of alpha decay[17-19] has been used most extensively for the calculation of decay constants, and therefore we will not consider other

Table I. Intensities for partial waves in alpha transitions to the favored band in ^{249}Bk (BFM).

Final state energy (keV)	Final state spin and parity	L=0(%)	L=2(%)	L=4(%)	$\sum$(%)	Expt.(%)
0	7/2+	79.6	10.0	0.127	89.7	90
41.7	9/2+	--	5.92	0.327	6.24	6.6
93.8	11/2+	--	0.88	0.267	1.15	0.85
155.8	13/2+	--	--	0.083	0.083	0.08
229.3	15/2+	--	--	0.0083	0.0083	0.014

(more exact but less extensive) direct numerical integrations of the coupled differential equations that have been performed.[20,21]

Mang's approach is essentially a nucleon overlap model in that the decay constant is proportional to the probability that the wave functions of the daughter nucleus and alpha particle are contained in the wave function of the parent nucleus. The shell model theory of alpha decay gives the decay constant as the product of a reduced width $\gamma^2_{I_i I_f L}$ which contains all information about the alpha formation process times a penetrability factor $P_L(\varepsilon)$ which accounts for the penetration of the predominantly coulombic barrier by the alpha particle. Thus

$$\lambda = \frac{1}{\hbar} \sum_{I_f L} P_L(\varepsilon)\ \gamma^2_{I_i I_f L} \tag{4}$$

where ε is the alpha particle kinetic energy.

The penetrability factor is usually calculated using the WKB approximation. The reduced width is given by

$$\gamma^2_{I_i I_f L} = \frac{\hbar^2}{2M} R_0 \left| g(I_i I_f L; R_0) \right|^2 \tag{5}$$

where $g(I_i I_f L; R_0)$ is a time-dependent probability amplitude measuring the probability that the wave function of the parent contains an alpha particle and a daughter of the specified quantum numbers at a relative distance R_0; it is related to the magnitude of the single particle wave functions at the nuclear surface.

Details about the calculation of transition probabilities are given by Poggenburg[22] and by Poggenburg, Mang and Rasmussen[23] (PMR). An abbreviated table for the main alpha transitions of ^{253}Es is given as Table II. The intensities were derived from the normalized transition probabilities given in Ref. 22. The shell model theory predicts relative phases of the partial waves in addition to wave amplitudes which are proportional to the square root of normalized transition probabilities.

The relative phases of the L-waves deserve some comment. As shown by Preston,[24] the relative phases can be obtained by the inward numerical integration of the coupled differential equations because of the requirement that the imaginary part of the wave function vanish at the nuclear surface for a quasi-stationary state. This condition permits two values for ϕ_L, one near zero and one near π. Brussard and Tolhoek[25] concluded that the phase shift due to penetration through the coulomb barrier would shift the S and D waves by less than 1%. Rasmussen and Hansen[21] estimated that because of the quadrupole coupling between the outgoing alpha particle and the rotational states of the daughter nucleus the D wave lags the S wave by 7° at infinity for the odd mass neighbors of ^{242}Cm.

The quadrupole phase shift is largest for a weak wave coupled to a strong wave, but fortunately in that case the interference term is small. Also the phase shift can be in either direction so the shifts may tend to cancel. We will assume that the waves are either exactly in phase or exactly out of phase and hence $\cos(\phi_L - \phi_{L'}) = \pm 1$.

Table IIA. Intensities and phases for partial waves in alpha transitions to the favored band in ^{249}Bk (Mang Shell-Model Theory).

I_f^π	S	D	G	I	$\sum$(%)	Expt.(%)
7/2+	-83.47	-8.94	0.079	0.0002	92.49	90
9/2+		-5.259	0.197	0.001	5.457	6.6
11/2+		-0.782	0.158	0.004	0.944	0.85
13/2+			-0.050	-0.004	0.054	0.08
15/2+			-0.0050	-0.0017	0.0067	0.014

Table IIB. Intensities and phases for partial waves in alpha transitions to the first excited rotational band in ^{249}Bk.

I_f^π	F	H	$\sum$(%)	Expt.(%)
3/2-	-0.39	-0.006	0.40	0.8
5/2-	-0.57	-0.008	0.58	0.7
7/2-	-0.33	-0.04	0.37	0.7

We now consider some solid-state aspects of this research. The similarity between the chemical properties of the actinides and lanthanides implies a similarity between the electronic structure of the actinides and the extensively studied lanthanides. This similarity was used to facilitate data interpretation.

For a free actinide ion J remains a good quantum number although L and S do not because the spin-orbit interaction causes a breakdown of Russell-Saunders coupling. An intermediate coupling calculation using extrapolated values for the electrostatic and spin-orbit interaction constants gave the Es^{3+} free ion wave function.[26] It is 79% $^5I_8$. In the lanthanides and actinides the spin-orbit interaction is stronger than the crystal field (CF) interaction which is in turn stronger than the hyperfine (hf) interaction. A CF of lower than cubic symmetry will partially or completely remove the $(2J+1)$-fold electronic degeneracy of the free ion giving a series of CF levels which are in turn split by the hf interaction.

The CF Hamiltonian can be written as

$$\mathcal{H}_{CF} = \sum_i \sum_{k,q} B_q^k \, (C_{\sim q}^{(k)})_i \qquad (6)$$

where B_q^k is a CF parameter which is proportional to the more familiar $A_k^q \langle r^k \rangle$ parameter. $C_{\sim q}^{(k)}$ is a tensor operator; the summation involving i is taken over all electrons of interest. For the rare earth ethylsulfates the only CF parameters that affect the electronic states are B_0^2, B_0^4, B_0^6 and B_6^6.

For N-electrons the non-relativistic magnetic hyperfine Hamiltonian for a free ion is[27]

$$\mathcal{H}_{mhf} = \frac{2\beta\beta_N\mu}{I} \sum_{i=1}^{N} \frac{\underset{\sim}{N}_i \cdot \underset{\sim}{I}}{r_i^3} + \frac{8\pi}{3} \sum_i \delta(r_i) \underset{\sim}{S}_i \cdot \underset{\sim}{I} \quad , \tag{7}$$

with $\underset{\sim}{N}_i = \underset{\sim}{l}_i - \sqrt{10}\,(\underset{\sim\sim}{s}\underset{\sim\sim}{C}^{(2)})_i^{(1)}$. The last term in Eq. (7) arises only if unpaired s-electrons are present or if core polarization effects are important.

For an ion at a site of axial symmetry the hf interaction can be described by a Spin Hamiltonian

$$\mathcal{H}_{hf} = AI_zS_z + B(I_xS_x + I_yS_y) + P(I_z^2 - \tfrac{1}{3}I(I+1)) \quad , \tag{8}$$

where A and B are magnetic hf interaction parameters and P is the quadrupole coupling constant. The hyperfine interaction can be adequately treated as a perturbation on the CF energy levels which were obtained by diagonalizing the combined electrostatic, spin-orbit and crystal field interaction matrices.

Again for an ion at a lattice site of axial symmetry the magnetic hyperfine interaction tensor has two components, one along the axis and one perpendicular to it. Then

$$A_\parallel = A = 4\beta\beta_N\mu \langle r^{-3} \rangle_{5f} \langle + | J_z | + \rangle \langle J \| N \| J \rangle / I \tag{9a}$$

$$A_\perp = B = 4\beta\beta_N\mu \langle r^{-3} \rangle_{5f} \langle + | J_x | - \rangle \langle J \| N \| J \rangle / I \quad . \tag{9b}$$

$|+\rangle$ and $|-\rangle$ represent the two components of the doubly degenerate CF state under consideration and

$$\langle J \| N \| J \rangle = \frac{\langle f^N S\ L\ J \| \sum_i N_i \| f^N S'L'J \rangle}{\langle f^N S\ L\ J \| \ J\ \| f^N S'L'J \rangle} \quad .$$

The discussion of the electric hyperfine interaction and the quadrupole coupling constant will be deferred until a future paper because the ^{253}Es data can be interpreted in terms of the magnetic hf interaction constants alone.

EXPERIMENTAL TECHNIQUES

The experimental work was performed independently by Navarro,[28] Frankel[8] and Soinski over a ten year period. Various modifications of technique and apparatus occurred; we report only those techniques used most recently.

The NES crystals were grown from saturated solutions at both room temperature and 277 K; growth at the lower temperature produced more perfect crystals. The crystals used weighed approximately 3 g. One face of the crystal was sanded flat at a 45° angle with respect to the crystalline c-axis. The radioactive trivalent ion in the form of either the nitrate or chloride salt was dissolved in several lambda ($1\lambda = 10^{-6}\ell$) of saturated NES solution. Two lambda of this solution were applied to the center of the sanded face and allowed to remain for 20 sec. before removal. The process was repeated until approximately 2×10^5 dpm of activity remained on the crystal. Those crystals exhibiting the highest saturation anisotropy were prepared with the fewest applications (ideally only one) of radioactive solution.

A NES crystal was mounted in a glass cryostat chamber shown in Fig. 3. The compressed manganous ammonium sulfate (MAS) pill serves as a "getter" for residual ^{4}He exchange gas. The chromium potassium alum (CA)-glycerine slurry cools upon adiabatic demagnetization to approximately the same temperature as NES and decreases the heat leak down the 2 mm diameter pyrex glass support rod. The nylon filament prevents the NES crystal from hitting the cryostat walls due to vibrations. The detectors are along and perpendicular to the NES c-axis. The error in positioning is estimated to be ± 2°. Because the second- and fourth-order Legendre polynomials are relatively flat at 0° and 90°, the errors introduced by misalignment are small.

Silicon semiconductor detectors were used to detect the alpha particles. Gold was evaporated on the front and back faces of 1 cm × 1 cm × 0.4 mm silicon wafers. An electrically conducting epoxy was used to fasten the detectors to molybdenum mounting strips and to secure a fine gold wire to the front electrode. Approximately 125 V reverse bias was applied to collect the charge carriers at the gold electrodes.

The final temperature reached after adiabatic demagnetization was determined from the initial values of H/T using the temperature scale of Blok et al.[29] The ratio of the initial magnetic field (measured with a rotating coil gaussmeter[30]) to the pumped helium bath temperature (measured with a dibutylphthalate filled manometer) determines the magnitude of the entropy of the electronic spin system and also the final temperature reached upon adiabatic demagnetization to zero applied magnetic field. Final temperatures measured in this manner are accurate to ± 6%.

Following adiabatic demagnetization several full spectrum "cold" counts were taken. The NES crystal was then warmed to the ^{4}He bath temperature (approximately 1 K) and a series of "warm" counts were taken for normalization. Because there is an anisotropic angular distribution at 1 K, these warm counts were renormalized to 4 K where the angular distribution is isotropic.

A typical pulse height spectrum is shown in Fig. 4. The alpha detectors used had an energy resolution (full width at half maximum) of 100 keV or better for 5.5 MeV alpha particles. The broadening of the peak shown in Fig. 4 is due to energy losses within the NES crystal. The effect of (Rutherford) scattering on the measured anisotropy was determined empirically by dividing typical spectra into several segments and by calculating the anisotropy of each segment. The

lowest energy segments should show the smallest anisotropy if large-angle scattering is important; but, within statistics the anisotropy was constant across each spectrum. However as a safeguard, the lowest 25% of the spectra were not used in calculating anisotropies. The ^{249}Bk daughter β^- activity contributed counts to the lowest part of the energy spectrum but no corrections were necessary because that part of each spectrum was excluded from analysis.

Solid angle correction factors were calculated by explicit numerical integration of the Legendre polynomials over both the finite source and detectors using a computer program written by Dr. William D. Brewer.

RESULTS

The experimental work on ^{253}Es was carried out in three sets of measurements, which we shall denote I^{28}, II^{8}, and III. Data from a good run in III are plotted in Fig. 5 and tabulated in Table III. The statistical accuracies are given in parentheses. In discussing these data, there are two rather distinct "figures of merit", which are best treated separately: the saturation values of $W(0)$ and $W(\pi/2)$ and their temperature dependences.

The observed saturation values of $W(0)$ and $W(\pi/2)$ are affected by the degree to which $^{253}Es^{3+}$ grows into Nd^{3+} lattice sites substitutionally, by scattering in the source crystal, and by the performance of the detectors. Values of $W(0)$ and $W(\pi/2)$ from I, II, and III are set out in Table IV. In I the "effect" as measured by the $\pi/2$ detector, i.e., $(1 - W(\pi/2))$ is relatively small: the same is true for the effect at the 0° detector, $(W(0) - 1)$, in II. In III, on the other hand, large effects are observed with both detectors. We interpret this to mean that III gave the most accurate saturation values for $W(0)$ and $W(\pi/2)$, because almost any error in a nuclear orientation experiment will act to reduce the effect observed. Inspection of the discrepancies in Table IV suggests that two kinds of errors were present in I and II. First, the smaller effect on even the "better" detector in each case suggests a source-preparation problem: perhaps the activity was too deep (leading to excessive scattering) or incompletely substituted into lattice sites. Secondly, the relatively large attenuation of the effect in the "poorer" detector in each case indicates something more grossly wrong either with that detector or with alpha emission in that direction (e.g., more scattering in the source in one direction). In III extreme care was taken to grow ^{253}Es only near the surface

Table III. Experimental ^{253}Es angular distribution as a function of the inverse temperature.

$1/T\ (K^{-1})$	$W(0)$	$W(\pi/2)$	$3 - W(0) - 2W(\pi/2)$
8.6(1)	1.566(27)	0.698(5)	0.038(28)
11.5(10)	1.712(22)	0.613(14)	0.062(30)
15.0	1.808(18)	0.578(16)	0.036(29)
19.2(5)	1.835(15)	0.544(14)	0.077(25)
25.5(10)	1.881(10)	0.543(5)	0.032(12)
31.2(2)	1.872(9)	0.533(7)	0.062(13)
40.8(13)	1.864(8)	0.524(6)	0.088(12)
49.1	1.864(8)	0.526(6)	0.084(12)
56.1	1.872(8)	0.518(8)	0.092(14)
74.0	1.880(8)	0.514(7)	0.092(13)
90.5	1.896(18)	0.520(4)	0.064(19)

Table IV. Saturation values for $W(\theta)$ after solid angle corrections.

Set	$W(0)$	$W(\pi/2)$	Reference
I	1.70	0.68	28
II	1.66	0.55	8
III	1.934	0.497	present work

of the crystal. Also the detectors and associated circuits were far more reliable than in I and II. The large effects observed with both detectors in series III were obtained with several sources. For these reasons we take the saturation values of $W(0)$ and $W(\pi/2)$ from series III as being characteristic of ^{253}Es in neodymium ethylsulfate.

The temperature dependences of $W(0)$ and $W(\pi/2)$ are affected by different variables than those that affect their saturation values. Immediately after demagnetization the small active volume of the NES crystal is warmed at an appreciable rate by radioactive heating. This can lead to a spurious apparent temperature dependence,[31] with the high-temperature points showing a reduced effect. The hyperfine structure constants derived in such cases are anomalously small. If gamma-ray distributions are studied the activity can be distributed throughout the NES crystal, and the temperature can be monitored through the magnetic susceptibility. For alpha-particle studies, however, the activity must be concentrated in a small volume on the surface, and the resulting intense self-heating can raise the local temperature well above that of the bulk crystal. Ironically, the stronger the source and the shallower its distribution in from the surface (two conditions condusive to reliable measurement of saturation values of $W(0)$ and $W(\pi/2)$), the worse will be the self-heating effect. Thus in our experiments, series I and II gave a temperature dependence in $W(0)$ and $W(\pi/2)$ characteristic of larger values of A (0.28 ± 0.03 cm^{-1}) than those that would be derived from series III ($A = 0.18 \pm 0.02$ cm^{-1}). The values of A obtained from several runs are given in Table V. The final adopted value of $A = 0.26 \pm 0.03$ cm^{-1} was decided from the entries in Table V on the basis of the above discussion.

Table V. Derived A values.

Series	Run	A (cm^{-1})	A/k (K)
I	1	0.28(2)	0.40(3)
	2	0.28	0.40
	3	0.25	0.36
II	1	0.28(3)	0.40(5)
	2	0.25(3)	0.36(4)
III	1	0.19(2)	0.28(3)
	2	0.17(2)	0.25(3)

Adopted value: $A = 0.26 \pm 0.03\ cm^{-1}$.

DISCUSSION

The curves shown in Fig. 5 are theoretical; the dashed and solid curves differ because different relative amplitudes were used for the partial waves. We sill discuss these curves and the saturation values of $W(0)$ and $W(\frac{\pi}{2})$ later; first we discuss the value for the hf interaction constant A and the derivation of the magnetic moment of ^{253}Es from A.

Baker and Bleaney[32] observed the paramagnetic resonance spectrum of Ho^{3+}, the $4f^{10}$ analogue of Es^{3+}, as a 1% impurity in a crystal of yttrium ethylsulfate. The ground CF state was a non-Kramers doublet characterized by $J_z = \pm 7$ with small admixtures of $J_z = \pm 1$ and ∓ 5. A singlet characterized by $J_z = +6, 0$, and -6 lay nearby in energy. The hf interaction constants for ^{165}Ho were $A = 0.334(1)\ cm^{-1}$, $B = 0.02\ cm^{-1}$, $P \approx 10^{-3}\ cm^{-1}$. The dominant term in the CF Hamiltonian is AI_zS_z, which results in alignment along the crystalline c-axis with the nuclear magnetic substate $I_z = \pm I$ lying lowest in energy.

The temperature dependence of $W(0)$ and $W(\pi/2)$ for ^{253}Es indicates that the AI_zS_z term is also dominant in the hfs of the lowest electronic CF state of Es^{3+} in the ethylsulfate lattice. It should therefore in principle be possible to derive a value for the nuclear magnetic moment, μ, of ^{253}Es. To do so, a description of the CF electronic ground state and a value for $\langle r^{-3} \rangle_{5f}$ are required in addition to the value for A.

Navarro et al.[7] used extrapolated values for the Es^{3+} CF parameters in the NES lattice. However, their extrapolation was based on Gruber's CF parameters for Am^{3+} in $LaCl_3$.[33] As pointed out by Conway,[34] Gruber misinterpreted

his data and therefore his CF parameters may be in error. The only reliable CF parameters for an actinide ion at a site of trigonal symmetry are those of Krupke and Gruber for Np^{3+} in $LaBr_3$.[35] The CF parameters for Es^{3+} in NES were estimated in two different ways. In the first method, we assumed that the A_k^q parameters are the same for analogous lanthanides and actinides and that the only difference is contained in the radial integrals. Using Hüfner's CF parameters for Ho^{3+} in holmium ethylsulfate[36] and ratios of radial integrals obtained from Hartree nonrelativistic wave functions without exchange,[37] the Es^{3+} CF parameters in wave numbers are $B_0^2 = 430$, $B_0^4 = -1380$, $B_0^6 = -1120$ and $B_6^6 = 960$. For Ho^{3+} in both holmium ethylsulfate[36] and $LaCl_3$ (ref. 38) the first excited state $J = 7$ is admixed into the ground state $J = 8$ by the CF interaction. Evaluation of $\mathcal{H}_{CF}$ for Es^{3+} with the inclusion of both the $J = 8$ and $J = 7$ wave functions[39] gave a singlet as the ground state. Because alignment would not occur if a singlet were lowest, B_0^2 was increased in magnitude in order to bring a doublet lowest in energy. Using $B_0^2 = 550 cm^{-1}$, the ground CF state is $0.939|\pm 7\rangle + 0.305|\pm 1\rangle + 0.153|\pm 5\rangle$.

A second estimate for the Es^{3+} CF parameters was obtained from the values for Ho^{3+} in HoES,[36] Np^{3+} in $LaBr_3$ (Ref. 35) (the CF parameters for Np^{3+} in the isoelectronic lattices $LaBr_3$ and $LaCl_3$ should be approximately the same),[40,41] and interpolated values for Pm^{3+} in $LaCl_3$.[42] The CF parameters obtained are $B_0^4 = -1440$, $B_0^6 = -760$ and $B_6^6 = 650$. B_0^2 is the most difficult parameter to obtain by this procedure because B_0^2 for Np^{3+} in $LaBr_3$ is negative as a result of a large ligand-(n = 5 shell) overlap exchange charge.[43] Again it was necessary to vary B_0^2 in order to get a doublet lowest. Using $B_0^2 = 600\ cm^{-1}$, the ground CF state is $0.967|\pm 7\rangle + 0.225|\pm 1\rangle + 0.120|\mp 5\rangle$.

The difficulties in extracting $\langle r^{-3} \rangle$ from experimental data have been discussed by several authors.[44-49] Because of the lack of experimental data for Es^{3+}, we take a value of $\langle r^{-3} \rangle_{5f} = 10.92$ au which was obtained using relativistic self-consistent Dirac-Fock wave functions.[50] The nuclear magnetic moment was calculated using Eq. (9a) which can be written as

$$\mu = \frac{AI}{4\beta\beta_N \langle r^{-3} \rangle_{5f} \langle + |J_z| + \rangle} \frac{\langle f^N S\ L\ J \| J \| f^N S'L'J \rangle}{\langle f^N S\ L\ J \| \Sigma N_i \| f^N S'L'J \rangle} . \qquad (10)$$

The two values for $|\mu|$ resulting from the two sets of CF parameters are 2.79(32) nm and 2.63(30) nm. The errors quoted in parenthesis reflect the statistical uncertainty in the value of A only. These values are substantially lower than the value of 4.9 nm previously reported[7] because of a change in the electronic ground CF state obtained with a different choice of CF parameters.

Using Nilsson's Eq. (24) (Ref. 51), a deformation parameter $\delta = 0.24$, $g_R = 0.3$ and $g_s^{eff} = 0.6\ g_s^{free}$, we calculate $\mu = 4.2$ nm. This value should be accurate to within a few nuclear magnetons. The major source of error in our value for the nuclear magnetic moment is the uncertainty of the ground crystal field state. Both of the predicted ground states have a large $J_z = \pm 7$ component which gives a small μ. No reasonable choice of CF parameters gave a coefficient for $|\pm 7\rangle$ of approximately 0.75 which would yield a moment of 4.2 nm. Therefore we report a nuclear magnetic moment $\mu = 2.7 \pm 1.3$ nm. The error reflects the statistical accuracy of the measured value of A and the uncertainties in the CF parameters and the radial integral $\langle r^{-3} \rangle_{5f}$.

Additional indirect measurements of the ^{253}Es nuclear magnetic moment have been made recently. Worden et al.[52] report a value of 5.1 (15) nm which was derived from the hfs observed in the ^{253}Es emission spectrum. The moment was calculated using the Goudsmit-Fermi-Segre formula to which large and uncertain relativistic corrections had to be made. N. E. Edelstein[53] reports a value of 3.5 (4) nm based on the analysis of the EPR spectrum of divalent ^{253}Es in CaF_2.[54]

Now we turn to an investigation of the saturation behavior of $W(0)$ and $W(\pi/2)$. The limiting values $B_2(1/T = \infty) = + 1.528$ and $B_4(1/T = \infty) = + 0.798$ are essentially realized in this experiment. Using the relative intensities and phases given by the Mang theory (Table II), the angular distribution function would be

$$W(\theta) = 1 + 0.576\, Q_2 B_2 P_2(\cos\theta) - 0.0248\, Q_4 B_4 P_4(\cos\theta) \quad , \qquad (11)$$

where Q_2 and Q_4 are solid angle correction factors. For the run summarized in Table III, $Q_2(0) = 0.946$, $Q_4(0) = 0.829$, $Q_2(\pi/2) = 0.962$ and $Q_4(\pi/2) = 0.877$. In calculating the Q_k's we assumed that the radioactivity was uniformly distributed throughout the spot. Since the activity would tend to concentrate at the center of the spot, the corrections may be too large; that is, the Q_k's should perhaps be larger in magnitude. The justification for dropping the $P_6(\cos\theta)$ term is that $B_6(1/T = \infty) = 0.174$ and $A_6 = -0.0025$. The 0.4% of the alpha decays not considered in the calculation of $W(\theta)$ were assumed to give the same angular distribution as the decays that were included.

Equation (11) is plotted as the dashed curve in Fig. 5; the fit to the saturation (lowest temperature) values of the data is poor. The experimental

result is

$$W(\theta) = 1 + 0.630(5)\, Q_2 B_2 P_2(\cos\theta) - 0.059(7)\, Q_4 B_4 P_4(\cos\theta) \quad . \qquad (12)$$

An examination of Table II reveals that the theoretical intensity to the 7/2 + level of ^{249}Bk is 2.5% larger than the observed intensity. Therefore the partial wave intensities for the alpha waves populating this level were changed in order to improve the fit to the data. Since the S wave contributes most of this intensity, the S wave intensity was decreased by 6%. The D wave intensity was increased by 22% (mainly to fit the $P_2(\cos\theta)$ term) and the G wave intensity was increased 220% (mainly to fit the $P_4(\cos\theta)$ term). The resulting angular distribution function would be

$$W(\theta) = 1 + 0.632\, Q_2 B_2 P_2(\cos\theta) - 0.0502\, Q_4 B_4 P_4(\cos\theta) \quad , \qquad (13)$$

which is plotted as the solid curve in Fig. 5. The fit to the lowest-temperature data is greatly improved, although it is not perfect. It is the best that we can do by changing the ^{253}Es ground state to ^{249}Bk ground state alpha particle transition probabilities only. Changing transition probabilities for decays to other levels in ^{249}Bk would not be instructive. The ability to fit the experimental data by varying the alpha partial wave intensities indicates that the angular distribution function is sensitive to the relative amplitudes of the partial waves and that quantitative information about the amplitudes can be obtained. The higher angular momentum waves are probably enhanced in intensity by the interaction between the outgoing alpha particle and the daughter nucleus. The S, D, and G-wave intensities that fitted the data best are given in Table VII.

The positive coefficient of $B_2P_2(\cos\theta)$ implies that the S and D partial waves are in phase. Enhanced alpha particle emission along the crystalline c-axis confirms the prediction of Hill and Wheeler. The negative coefficient of $B_4P_4(\cos\theta)$ implies that the S and G waves are out of phase confirming the prediction of Mang and Rasmussen.[18] That the coefficient of $B_4P_4(\cos\theta)$ is negative is illustrated in Fig. 6. If the solid angle correction factors are unity (point source and point detectors), $3 - W(0) - 2\,W(\pi/2) = -7/4\,A_4B_4$; however, because they are not unity, a small component proportional to $P_2(\cos\theta)$ enters. Clearly the coefficient of $B_4P_4(\cos\theta)$ is negative. The dashed and solid lines are theoretical assuming the intensities given by PMR and the modified PMR intensities, respectively. Again the modified intensities give the better fit to the data.

Using the intensities predicted by BFM as given in Table I and taking the S and D waves as in phase and the S and G waves as out of phase, as required by the experimental results, the angular distribution function would be

$$W(\theta) = 1 + 0.594\,Q_2B_2P_2(\cos\theta) - 0.006\,Q_4B_4P_4(\cos\theta) \quad . \qquad (14)$$

The saturation anisotropies in this case are $W(0,1/T \to \infty) = 1.854$ and $W(\pi/2,1/T \to \infty) = 0.561$, giving poor agreement with experiment. For convenience we have tabulated the experimental and theoretical values of A_2 and A_4 in Table VIII.

Table VII. Relative alpha partial wave intensities for the decay of ^{253}Es.

	This work	Mang theory	BFM theory
a_0^2	1.000	1.000	1.000
a_2^2	0.216	0.179	0.211
a_4^2	0.0084	0.0058	0.010

Table VIII. Coefficients A_2 and A_4 for the ^{253}Es in NES angular distribution function $W(\theta) = 1 + A_2Q_2B_2P_2(\cos\theta) + A_4Q_4B_4P_4(\cos\theta)$.

	A_2	A_4	$W(0, 1/T \to \infty)$	$W(\pi/2, 1/T \to \infty)$
Experiment	0.630(5)	-0.059(7)	1.872(7)	0.521(4)
BFM(S and G waves out of phase)	0.594	-0.006	1.854	0.561
BFM(S and G waves in phase)	0.698	+0.138	2.102	0.523
Mang theory(S and G waves predicted to be out of phase)	0.576	-0.0248	1.816	0.570
Mang theory but with modified partial wave intensities	0.632	-0.0502	1.880	0.522

An alpha-gamma angular correlation experiment[55] on ^{233}U in 1 N $HClO_4$ solution also indicated that the BFM theory underestimates the G wave intensity. Within statistical accuracy the angular correlation results are consistent with the Mang theory intensities. Chasman and Rasmussen[6] have considered the effect of quadrupole coupling between the outgoing alpha wave and the daughter nucleus on the relative intensities predicted by BFM. They concluded that the D wave intensity is enhanced by 20% for ^{233}U. A similar correction should apply to ^{253}Es and would give better agreement between theory and experiment. No estimate has been made of G wave intensity enhancement, which we have found to be substantial.

CONCLUSION

Es^{3+} and Ho^{3+} have similar electronic structure as is evidenced by their having the same nuclear orientation mechanism. Magnetic hyperfine splitting in both cases results from the interaction between the orbital and spin moments of the unpaired f-electrons and the nuclear magnetic dipole moment. The ions are of predominantly $^5I_8$ character, and, as expected, the Es^{3+} electronic wave function contains less ^5I character than the Ho^{3+} wave function.

Mang's shell model alpha decay theory successfully predicts the relative phases of the alpha partial waves. The theoretical relative transition probabilities are not consistent with the experimentally determined wave amplitudes, but it is not clear whether the defect is in the theory itself or in the calculations of Poggenburg. The Fröman matrix method was used in calculating the barrier penetration factors. However, this method is not too good for solving coupled equations for a weak partial wave coupled to a strong wave. Clearly what is needed is a coupled-channel barrier penetration calculation such as the one performed by Rasmussen and Hansen for ^{242}Cm. Such a calculation also gives the quadrupole coupling phase shifts and hence would remove the need for assuming that the alpha partial waves differ in phase by exactly 0 or π.

The disagreement between our value for the ^{253}Es magnetic moment and other experimental values points to the need for additional ESR or optical spectrometric studies of salts of the actinides. A re-examination of the Am^{3+} in $LaCl_3$ spectra would be especially interesting to us. It should be pointed out that the trivalent lanthanide ion crystal spectra have been analyzed at various levels of sophistication and therefore the extrapolation from the Np^{3+} CF parameters to those for Es^{3+} on the basis of reported behavior in the lanthanides is open to question.

ACKNOWLEDGMENTS

Professor J. O. Rasmussen originally suggested this research and encouraged its completion. Dr. B. B. Cunningham and his co-workers supplied the separated radioactive isotopes used in this research. We are grateful to Dr. N. E. Edelstein for many helpful discussions and for the use of several computer programs.

FOOTNOTES AND REFERENCES

*Work performed under the auspices of the U. S. Atomic Energy Commission.

†Permanent address: National Magnet Laboratory, Massachusetts Institute of Technology, Cambridge, Massachusetts.

††Permanent address: Philippine Atomic Research Center, Diliman, Quezon City, The Philippines.

1. J. A. Spiers, Nature 161, 807 (1948).
2. D. L. Hill and J. A. Wheeler, Phys. Rev. 89, 1102 (1953).
3. L. D. Roberts, J. W. T. Dabbs, and G. W. Parker, Oak Ridge National Laboratory Report ORNL-2204, p. 60 (1956) (unpublished).
4. J. W. T. Dabbs, L. D. Roberts, and G. W. Parker, Oak Ridge National Laboratory Report ORNL-2430, p. 50 (1958) (unpublished) and Physica 24, S69 (1958).
5. S. H. Hanauer, J. W. T. Dabbs, L. D. Roberts, and G. W. Parker, Phys. Rev. 124, 1512 (1961).
6. R. R. Chasman and J. O. Rasmussen, Phys. Rev. 115, 1257 (1959).
7. Q. O. Navarro, J. O. Rasmussen, and D. A. Shirley, Phys. Letters 2, 353 (1962).
8. Richard Barry Frankel, Lawrence Radiation Laboratory Report UCRL-11871 (1964) (unpublished).
9. E. Ambler, Prog. in Cryogenics 2, 1 (1960).
10. Louis D. Roberts and J. W. T. Dabbs, Ann. Rev. Nucl. Sci. 11, 175 (1961).
11. R. J. Blin-Stoyle and M. A. Grace, Handbuch der Phys. 42, 555 (1957).
12. S. R. de Groot, H. A. Tolhoek and W. J. Huiskamp, in Alpha-, Beta-, and Gamma-Ray Spectroscopy, 2nd Ed., ed. K. Siegbahn (North-Holland Publishing Co., Amsterdam, 1965) p. 1199.

13. David A. Shirley, Ann. Rev. Nucl. Sci. 16, 89 (1966).

14. A. Bohr, P. O. Fröman and B. R. Mottelson, Kgl. Dans. Vid. Selsk Mat. Fys. Medd. 29, No. 10 (1955).

15. H. J. Mang, J. K. Poggenburg, and J. O. Rasmussen, Nucl. Phys. 64, 353 (1965).

16. C. M. Lederer, J. M. Hollander and I. Perlman, Table of Isotopes, 6th Ed. (John Wiley and Sons, Inc., New York, 1967).

17. H. J. Mang, Z. Physik 148, 582 (1957); Phys. Rev. 119, 1069 (1960), and Ann. Rev. Nucl. Sci. 14, 1 (1964).

18. H. J. Mang and J. O. Rasmussen, Mat. Fys. Skr. Dan. Vid. Selsk 2, No. 3 (1962).

19. H. D. Zeh and H. J. Mang, Nucl. Phys. 29, 529 (1962).

20. John O. Rasmussen and Benjamin Segall, Phys. Rev. 103, 1298 (1956).

21. John O. Rasmussen and Eldon R. Hansen, Phys. Rev. 109, 1656 (1958).

22. John Kenneth Poggenburg, Jr., Lawrence Radiation Laboratory Report UCRL-16187 (1965) (unpublished).

23. J. K. Poggenburg, H. J. Mang, and J. O. Rasmussen, Phys. Rev. 181, 1697 (1969).

24. M. A. Preston, Physics of the Nucleus (Addison-Wesley Publishing Co., Inc., Reading, Pa., 1962) p. 369.

25. P. J. Brussard and H. A. Tolhoek, Physica 24, 233 (1958).

26. The input parameters in wavenumbers were $E^1 = 5300$, $E^2 = 23$, $E^3 = 480$, $\zeta = -3700$, $\alpha = 78$, $\beta = -250$, $\gamma = -0.1$. The configuration interaction parameters α, β and γ are discussed by W. T. Carnall, P. R. Fields and

K. Rajnak, J. Chem. Phys. 49, 4424 (1968).

The Es^{3+} free ion wave function obtained is

$$0.8880|^5 I_{20}) + 0.2073|^3 K_{21}) - 0.3846|^3 K_{20})$$

$$-0.0908|^3 L_{21}) - 0.0287|^3 M_{30}) + 0.1016|^1 L_{22})$$

$$+0.0341|^1 L_{21}) \quad .$$

The lower subscripts are the U quantum numbers which label the irreducible representations of the group G_2.

27. Brian G. Wybourne, Spectroscopic Properties of the Rare Earths (Interscience Publishers, New York, 1965).

28. Quirino Ole Navarro, Lawrence Radiation Laboratory Report UCRL-10362 (1962) (unpublished).

29. J. Blok, D. A. Shirley, and N. J. Stone, Phys. Rev. 143, 78 (1966).

30. Rotating coil gaussmeter, model 203A, manufactured by George Associates, Berkeley, California.

31. Morton Kaplan, J. Blok and D. A. Shirley, Phys. Rev. 184, 1177 (1969).

32. J. M. Baker and B. Bleaney, Proc. Phys. Soc. (London) A68, 1090 (1950); and Proc. Roy. Soc. (London) A245, 156 (1958).

33. J. B. Gruber, J. Chem. Phys. 35, 2186 (1961).

34. John G. Conway, J. Chem. Phys. 40, 2504 (1964).

35. William F. Krupke and John B. Gruber, J. Chem. Phys. 46, 542 (1967).

36. S. Hüfner, Z. Physik 169, 427 (1962).

37. Allen C. Larson and James T. Waber, Los Alamos Scientific Laboratory Report LA-4297 (1969) (unpublished).

38. Katheryn Rajnak and William F. Krupke, J. Chem. Phys. 46, 3532 (1967).

39. For the J = 7 excited state we used a truncated wave function given by

$$0.4279|^5 I_{20}) - 0.3363|^3 K_{21}) + 0.5848|^3 K_{20}) + 0.3750|^3 L_{21}) \quad .$$

For the J = 8 ground state we also used a truncated wave function and considered only the quintet and the triplet states.

40. Eugene Y. Wong and Isaac Richman, J. Chem. Phys. 36, 1889 (1962).

41. In $LaCl_3$ a slightly smaller B_6^6/B_0^6 ratio is expected with both B_6^6 and B_0^6 being larger than in $LaBr_3$. B_0^4 should be slightly smaller in $LaCl_3$ than in $LaBr_3$. Private communication, D. J. Newman, 1970.

42. The experimentally determined CF parameters of rare earths in $LaCl_3$ are tabulated by M. M. Curtis, D. J. Newman and G. E. Stedman, J. Chem. Phys. 50, 1077 (1969).

43. S. S. Bishton, M. M. Ellis, D. J. Newman and J. Smith, J. Chem. Phys. 47, 4133 (1967).

44. A. J. Freeman and R. E. Watson, Phys. Rev. 127, 2058 (1962).

45. G. K. Woodgate, Proc. Roy. Soc. (London) A293, 117 (1966).

46. B. Bleaney, Proc. Third Intern. Cong. on Quantum Electronics, Paris, 1963, (Columbia University Press, New York, 1964) and Hyperfine Interactions, eds. A. J. Freeman and R. B. Frankel, Chap. 1, (Academic Press, New York, 1967).

47. P. G. H. Sandars and J. Beck, Proc. Roy. Soc. (London) A289, 97 (1965).

48. R. E. Watson and A. J. Freeman, Hyperfine Interactions, eds. A. J. Freeman and R. B. Frankel, Chap. 2, (Academic Press, New York, 1967).

49. P. G. H. Sandars and B. Dodsworth, Hyperfine Interactions, eds. A. J. Freeman and R. B. Frankel, Chap. 2, (Academic Press, New York, 1967).

50. We are grateful to Dr. Joseph B. Mann of the Los Alamos Scientific Laboratory for communicating these results to us prior to publication.

51. S. G. Nilsson, Kgl. Dans. Vid. Selsk Mat. Fys. Medd. 29, No. 16 (1955).

52. E. F. Worden, R. G. Gutmacher, R. W. Lougheed, J. G. Conway and R. J. Mehlhorn, J. Opt. Soc. Amer., to be published.

53. N. Edelstein, private communication, 1970.

54. N. Edelstein, John G. Conway, D. Fujita, W. Kolbe and R. McLaughlin, J. Chem. Phys. Letters, to be published.

55. J. M. R. Hutchinson, Phys. Rev. 157, 1093 (1967).

FIGURE CAPTIONS

Fig. 1. Representation of the total (nuclear plus coulomb) potential of a prolately deformed nucleus, of major (minor) radius $r_a(r_b)$, showing that alpha particles emitted from polar regions must tunnel through a barrier that is both lower and thinner than at the equator.

Fig. 2. Partial decay scheme for ^{253}Es adapted from Ref. 16 . The alpha particle populations are shown in parenthesis.

Fig. 3. Experimental chamber for nuclear orientation studies of alpha emitting isotopes.

Fig. 4. Typical axial counter pulse height spectrum for ^{253}Es in NES. The cold spectrum was taken at 0.011 K and the warm spectrum at 1 K.

Fig. 5. Experimental angular distribution of ^{253}Es in NES as a function of the inverse temperature. The curves shown are theoretical based on different estimates for the relative intensities of the alpha partial waves.

Fig. 6. Temperature dependence of the (negative) coefficient of the $P_4(\cos\theta)$ term in the ^{253}Es angular distribution function. The curves shown are theoretical based on different estimates for the relative intensities of the alpha partial waves.

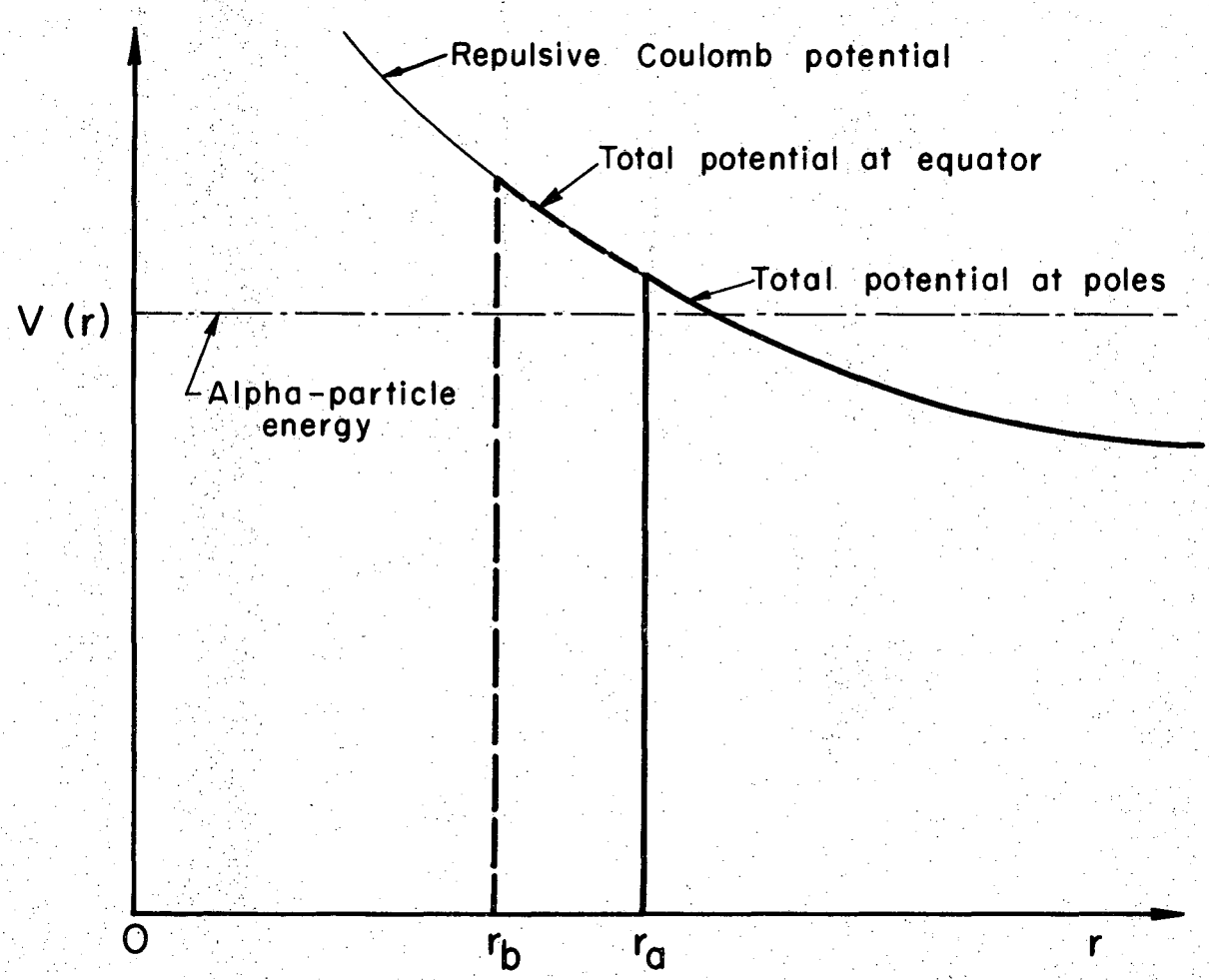
Repulsive Coulomb potential
Total potential at equator
Total potential at poles
V (r)
Alpha-particle energy
O
r_b
r_a
r
MUB-10078

Fig. 1

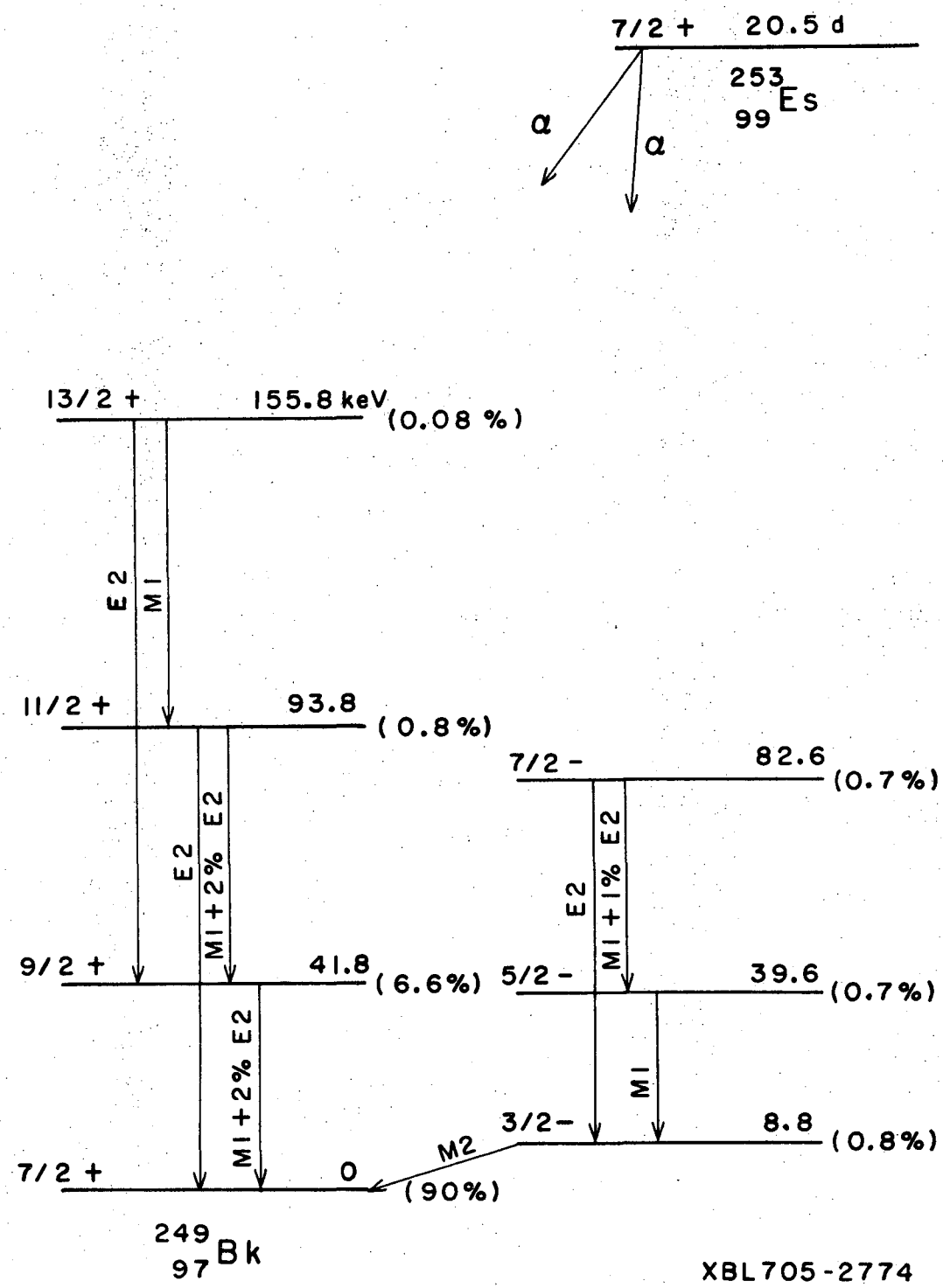
7/2 + 20.5 d
253 99 Es
α
α
13/2 + 155.8 keV (0.08 %)
E2
M1
11/2 + 93.8 (0.8%)
E2
M1+2% E2
9/2 + 41.8 (6.6%)
M1+2% E2
7/2 + 0
249 97 Bk
7/2 - 82.6 (0.7%)
E2
M1+1% E2
5/2 - 39.6 (0.7%)
M1
3/2 - 8.8 (0.8%)
M2
(90%)
XBL705-2774

Fig. 2

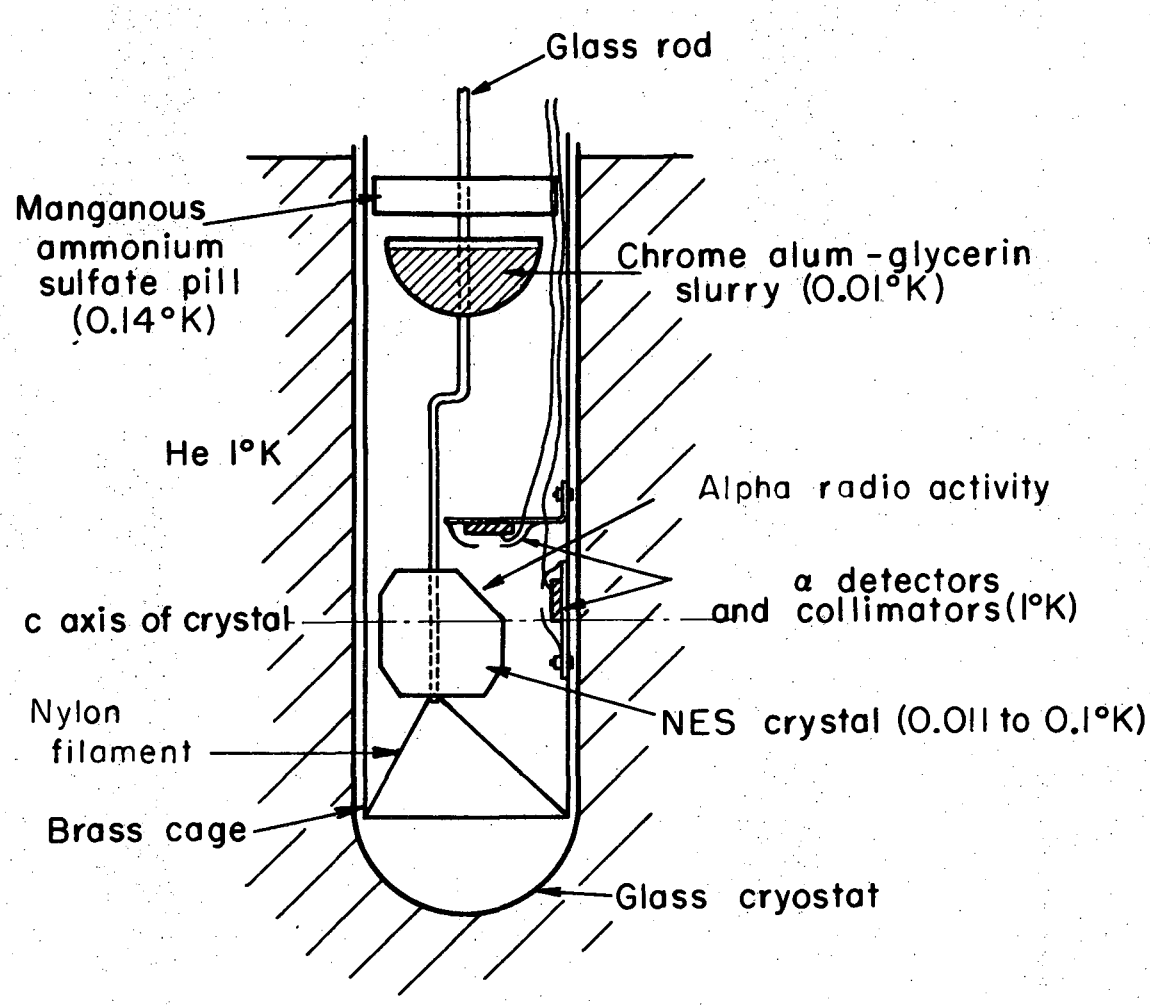
Glass rod
Manganous ammonium sulfate pill (0.14°K)
Chrome alum-glycerin slurry (0.01°K)
He 1°K
Alpha radio activity
α detectors and collimators (1°K)
c axis of crystal
Nylon filament
NES crystal (0.011 to 0.1°K)
Brass cage
Glass cryostat
MUB-2999

Fig. 3

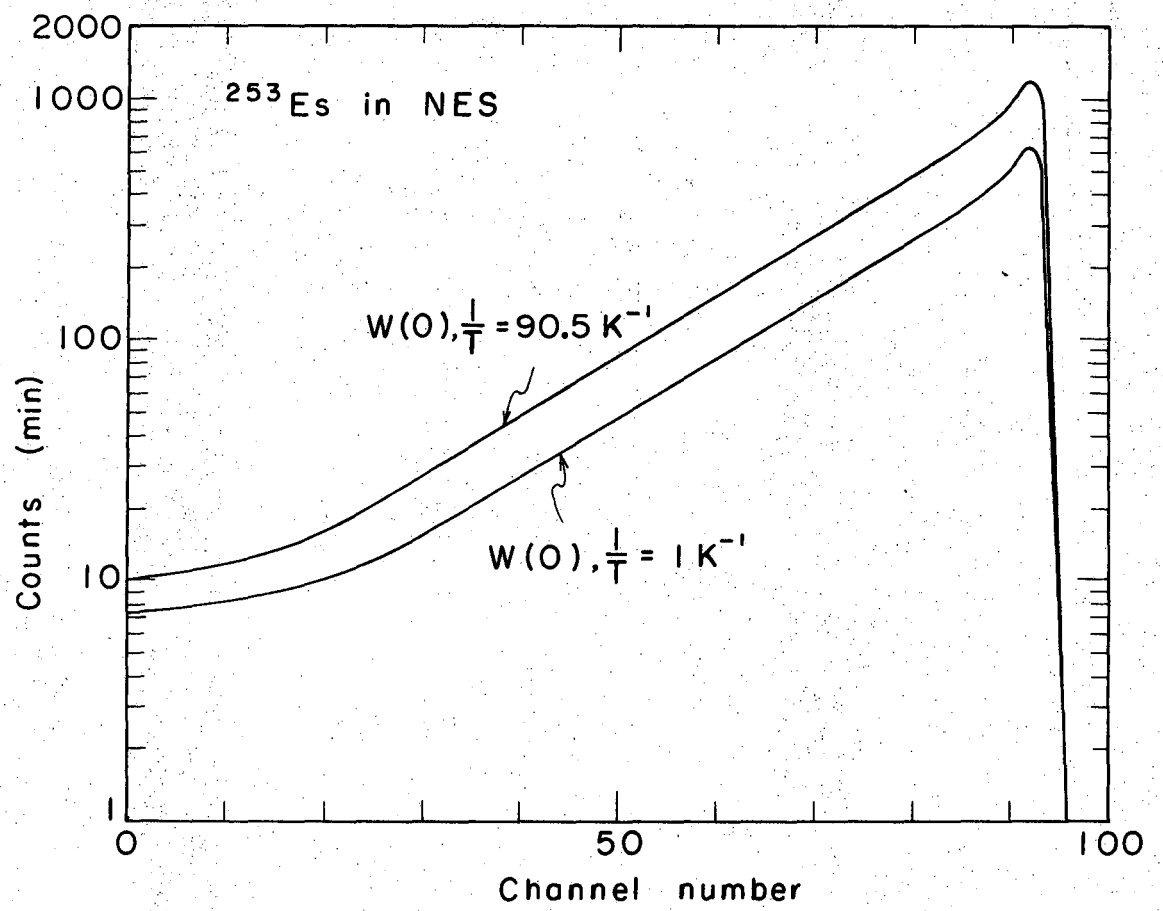
2000
1000
100
10
1
Counts (min)
^{253}Es in NES
W(0), $\frac{1}{T}$ = 90.5 K^{-1}
W(0), $\frac{1}{T}$ = 1 K^{-1}
0
50
100
Channel number
XBL705-2773

Fig. 4

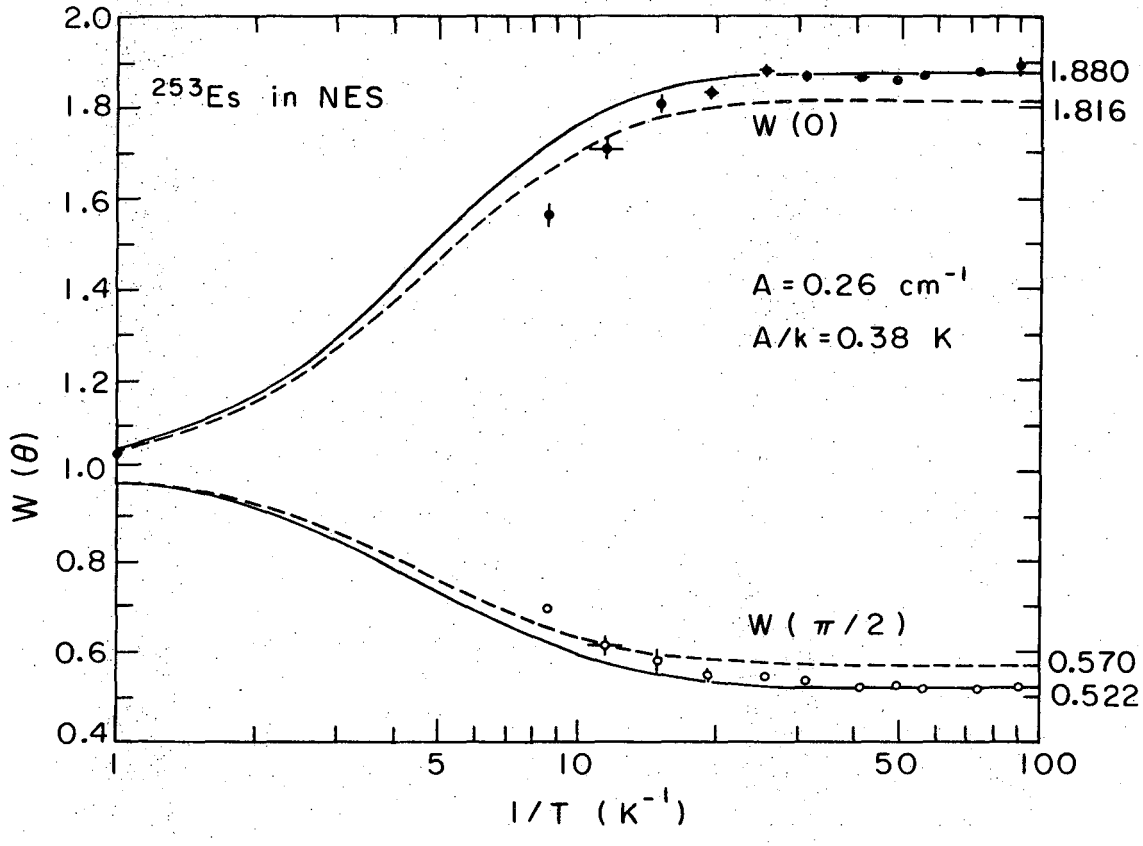

XBL705-2772

Fig. 5

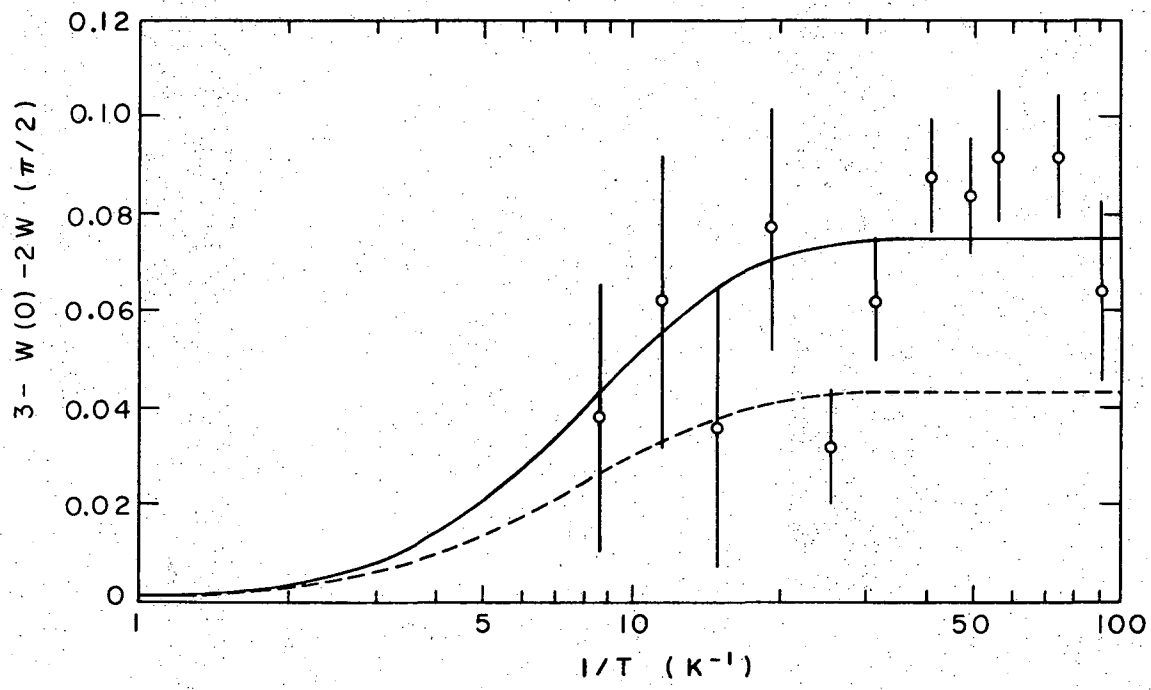

Fig. 6

LEGAL NOTICE

TECHNICAL INFORMATION DIVISION
LAWRENCE RADIATION LABORATORY
UNIVERSITY OF CALIFORNIA
BERKELEY, CALIFORNIA 94720